Journal of Hydrology 619 (2023) 129297

Contents lists available at ScienceDirect

Journal of Hydrology

journal homepage: www.elsevier.com/locate/jhydrol

Research papers

# Multi-model analysis of historical runoff changes in the Lancang-Mekong River Basin – Characteristics and uncertainties

Yuxin Li [a,1], Aifang Chen [a,1], Ganquan Mao [a], Penghan Chen [a], Hao Huang [a], Hong Yang [b], Zifeng Wang [a], Kai Wang [a], He Chen [a], Ying Meng [a], Rui Zhong [a], Pengfei Wang [a], Hong Wang [a], Junguo Liu [a,c,*]

[a] School of Environmental Science and Engineering, Southern University of Science and Technology, 518055, China
[b] Department of Systems Analysis, Integrated Assessment and Modelling, Swiss Federal Institute for Aquatic Science and Technology (Eawag), 8600, Switzerland
[c] School of Water Conservancy, North China University of Water Resources and Electric Power, Zhengzhou 450046, People's Republic of China

ARTICLE INFO

This manuscript was handled by Andras Bardossy, Editor-in-Chief, with the assistance of Ashish Sharma, Associate Editor

*Keywords:*
High flow
ISIMIP
Low flow
Multi-model
Uncertainty

ABSTRACT

Runoff changes are critical to the sustainable water resource in the Lancang-Mekong River Basin (LMRB). Changes in the LMRB's runoff over the past decades are unclear because of inadequate streamflow observations. The advancement of global hydrological models (GHMs) has facilitated the understanding of runoff change worldwide. However, it is required to evaluate the performance of GHMs in simulating historical runoff change in the LMRB before assessing the runoff changes. This study aims to conduct a multi-model analysis of temporal-spatial changes in runoff in the LMRB for 1971–2010 using ten GHMs from the Inter-Sectoral Impact Model Intercomparison Project (ISIMIP) and evaluate the corresponding uncertainties among models. Results show that the model ensemble mean has the best performance than the individuals when compared with the reference data. Based on the model ensemble mean, large spatial heterogeneity of runoff is found in the LMRB, with an overall slightly positive trend (8.03%). Besides, the models perform better in estimating the trends of high flow than low flow. As to the trend of runoff in the wet and dry seasons, about 32% (70%) of the basin became drier (wetter) in the dry (wet) season. Meanwhile, 17% of the basin has experienced a trend of drier dry seasons and wetter wet seasons. Overall, our results highlight the uncertainty of the runoff changes in the LMRB in the low flow simulation, particularly requiring more attention in future model improvement. The complex change patterns of the runoff suggest the importance of accurate runoff observations and projections for better water management.

## 1. Introduction

Surface runoff constitutes a significant component of the available water resources strongly associated with regional socio-economic development (Wu et al., 2017). The non-public available streamflow data for most land areas hampers the investigation of runoff changes (Asadieh et al., 2016). Global hydrological models (GHMs) development has advanced rapidly over the past decades, which simulates satisfactory land surface hydrologic dynamics of continental-scale river basins, and provides runoff at the grid level (Gosling and Arnell, 2011). Employing the hydrological models makes the investigation of spatiotemporal changes to runoff possible. It further improves our understanding of regional hydrological cycle changes, which could support water resource management, protection, and sustainable use (Shan et al., 2021).

Despite the significant advancement of GHMs, the available hydrological simulation outputs are of discrepancies because they are simulated by unique hydrological models, which have different representations of hydrological processes (Sood and Smakhtin, 2015). In addition, different climate-forcing inputs could also bring discrepancies in the simulations (Hattermann et al., 2018). Intercomparisons of the simulations from the GHMs are thus needed before further evaluating the hydrological analysis. Model inter-comparison projects like the Inter-Sectoral Impact Model Intercomparison Project (ISIMIP) (Warszawski et al., 2014) have made it possible to evaluate the GHMs simulations and apply the outputs in global impact studies, thereby providing

* Corresponding author at: School of Environmental Science and Engineering, Southern University of Science and Technology, No. 1088, xueyuan Rd., Xili, Nanshan District, Shenzhen, Guangdong 518055, China.
*E-mail address:* junguo.liu@gmail.com (J. Liu).
[1] Y.L., and A.C. contributed equally to this work.

https://doi.org/10.1016/j.jhydrol.2023.129297
Received 25 March 2022; Received in revised form 11 February 2023; Accepted 15 February 2023
Available online 18 February 2023

frameworks for consistent assessments of the terrestrial water cycle (Giuntoli et al., 2015). Some studies have investigated the runoff trends using multi-model approaches (Hoang et al., 2016; Thompson et al., 2013). Milly et al. (2005) showed that an ensemble of 12 climate models exhibits qualitative and statistically significant skill in simulating observed regional patterns of twentieth-century multidecadal changes in streamflow. Stahl et al. (2012) tested whether the white space on maps of observed runoff trends in Europe could be filled using estimates of an ensemble of eight GHMs. They showed that the ensemble mean overall provided the best representation of trends in the observations. Najafi and Moradkhani (2015) analyzed the extreme runoff by the multi-model ensemble of eight regional climate models, and found that the merged signal generally outperforms the best individual signal. Marx et al. (2017) investigated how the hydrological low flows were affected under different levels of future global warming in rivers using a multi-model ensemble of 45 hydrological simulations, and they concluded that climate change studies focusing on river low flows should employ large multi-model ensembles to provide a comprehensive analysis of model uncertainty.

As one of Asia's largest transboundary river basins, the Lancang-Mekong River Basin (LMRB, Fig. 1) plays a vital role in economic development in Southeast Asia (Liu et al., 2021). The fishery, agriculture, and hydropower sectors along the river are highly dependent on this commonly shared water resource (Yun et al., 2020). Recent studies have shown increased magnitudes and frequencies of floods and droughts in the LMRB in the past decades (Hoang et al., 2016; Lyon et al., 2017), which will be further intensified under future climate change (Eastham et al., 2008; Hoang et al., 2016; Lauri et al., 2012; Västilä et al., 2010). However, previous multi-model studies in the LMRB mainly focused on changes in future runoff (including drought and floods) under the projected impact of climate change (Hasson et al., 2016; Hoang et al., 2019; Lauri et al., 2012), a multi-model analysis of historical changes in runoff in the LMRB has not been conducted. The study of historical runoff regime changes would provide useful information regarding the temporal and spatial evolution of runoff in response to climate change (Bawden et al., 2015). Therefore, an assessment of historical changes in the runoff regime of the LMRB is necessary to provide valuable information on water availability for subsequent management.

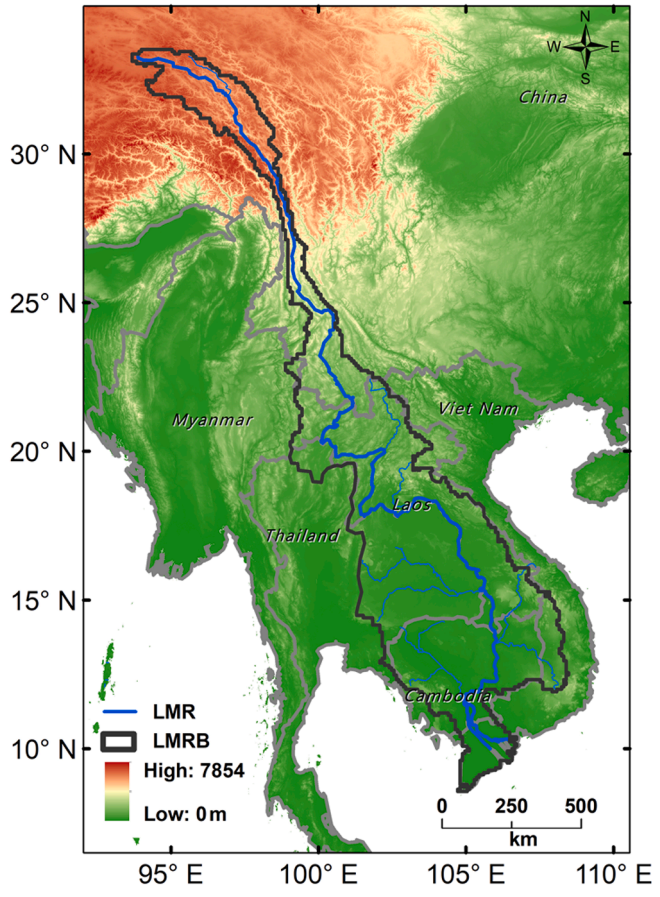


**Fig. 1.** Terrain and the location of the Lancang-Mekong River Basin (LMRB).

Although Chen et al. (2021) have evaluated the performance of ISIMIP models in simulating Lancang-Mekong River discharges, it has shown a systematic underestimation at low percentiles of discharge due to the models' routing scheme. Therefore, to further explore the performance and associated uncertainties of ISIMIP models in simulating LMRB runoff, the temporal-spatial runoff regime changes in the LMRB during 1971–2010 were comprehensively investigated. Our key objectives include the following: (1) to assess the runoff regime changes concerning different hydrological indicators using multi-model simulations; (2) to estimate the associated uncertainties among models in addition to the spatial characteristics of runoff regime changes; (3) to identify "hot spots" of runoff change in the LMRB. Although traditional uncertainty analyses have been conducted (in a rather narrow sense) by considering contributions based on certain metrics (such as the coefficient of variation) (Phi Hoang et al., 2016), multiple metrics have rarely been quantified. Thus, our study quantifies the uncertainties in runoff trend detection using three different metrics, and the results provide a better understanding of the model performances. In addition, a deeper understanding of the past runoff regime characteristic changes and uncertainties relating to multi-model approaches can also assist in improving projections of future hydrological regime changes in the LMRB.

## 2. Materials and methods

### 2.1. Materials

In this study, the simulated daily runoff data from ten state-of-the-art GHMs (CLM4, DBH, H08, LPJmL, MATSIRO, MPI-HM, PCR-GLOBWB, VIC, WaterGAP2, and WAYS) are used to analyze changes in the runoff regime within the LMRB during 1971–2010. All the selected models were used in the second phase of the ISIMIP (ISIMIP2a) (Warszawski et al., 2014). All models were driven by the same climate forcing (Global Soil Wetness Project Phase 3 data, hereafter abbreviated as GSWP3) using a spatial resolution of 0.5° from 1 January 1971 to 31 December 2010 on a continuous run on the daily scale. The GSWP3 dataset was generated based on the 20th Century Reanalysis Project and has been widely used in several studies conducting hydrological simulations (Masaki et al., 2017; Tangdamrongsub et al., 2018; Veldkamp et al., 2017). The WaterGAP and WAYS models were calibrated prior to the hydrological simulation (Alcamo et al., 2003; Mao and Liu, 2019). The other eight models were not calibrated specifically for the ISIMIP2a simulations, and their default model parameters were therefore used in the runoff simulations. None of the selected models have considered the effects of water management and other human activities on the water system. Though many of them shared similar structures and parameterizations, all models were treated as independent. For example, some were similar concerning their fundamental approach to simulating evapotranspiration, representing water exchanges in soil across the basin, and modeling snow melting. The primary differences in the models concerning simulating land-surface hydrological processes are presented in Table 1. Detailed descriptions of the models applied in this work are provided by references associated with each model cited in the table.

The International Satellite Land Surface Climatology Project Initiative II University of New Hampshire/Global Runoff Data Centre (ISLSCP II UNH/GRDC, hereafter referred to as UNH-GRDC) composite monthly runoff data are available at a spatial resolution of 0.5° for 1986–1995,

**Table 1**
Description of ten evaluated global hydrological models.

| Model | Snow melt scheme | Evapotranspiration scheme | Number of soil layers | Spatial schematization | Number of parameters | Reference |
|---|---|---|---|---|---|---|
| CLM4 | Physically based snow module | Monin-Obukhov Similarity Theory | 15 | Fully-distributed | >50 | (Lawrence et al., 2011) |
| DBH | Energy balance method | Energy balance model | 3 | Fully-distributed | 15 | (Tang et al., 2006) |
| H08 | Energy balance method | Bulk approach | 1 | Fully-distributed | – | (Hanasaki et al., 2008) |
| LPJmL | Degree-day method | Priestley–Taylor | 6 | Fully-distributed | – | (Gerten et al., 2004) |
| MATSIRO | Energy balance method | Monin-Obukhov Similarity Theory | 13 | Fully-distributed | 16 | (Takata et al., 2003) |
| MPI-HM | Degree-day method | Penman-Monteith | 1 | Fully-distributed | – | (Stacke and Hagemann, 2012) |
| PCR-GLOBWB | Degree-day method | Hamon | 2 | Fully-distributed | 43 | (van Beek et al., 2011) |
| VIC | Energy balance method | Penman-Monteith | 3 | Semi-distributed | 22 | (Liang et al., 1994) |
| WaterGAP2 | Degree-day method | Priestley–Taylor | 1 | Fully-distributed | 36 | (Alcamo et al., 2003) |
| WAYS | Degree-day method | Penman-Monteith | 1 | Fully-distributed | 13 | (Mao and Liu, 2019) |

Note: "-" indicates the number of parameters in the model is not explicitly specified.

which represents the composite runoff data based on the water balance model runoff estimates and assimilates of observed discharge at gauge stations. The spatial characteristics of the water balance are preserved but constrained by the records observed at stations (Fekete et al., 2011). The UNH-GRDC data also represents a standard dataset used in the ISIMIP2a for model validation (Warszawski et al., 2014). Therefore, the UNH-GRDC was employed as reference data to evaluate the performances of model simulations in the study area.

## 2.2. Methods

A framework for multi-model analyses is compiled to investigate the runoff regime changes in the LMRB when considering both spatiotemporal characteristics and uncertainties, which are outlined in Fig. 2 and detailed in the following sections:

1. Evaluate the model performance in replicating the temporal and spatial patterns of the reference runoff data using seven commonly used metrics.
2. Conduct trend detection for six hydrological indicators first at the basin scale and then grid scale to demonstrate the temporal and spatial patterns of runoff regime changes in the LMRB for 1971–2010.
3. Quantify the uncertainties in runoff trend detection for each hydrological indicator using three metrics to explore confidence in the trend signal for runoff at different magnitudes over the study period.
4. Analyze runoff regime changes in the dry (November–May) and wet (June–October) seasons. The regions where runoff increased in the wet season and decreased in the dry season were highlighted.

### 2.2.1. Metrics used in model performance evaluation

Before investigating runoff regime changes, the models applied in this study are evaluated against the reference runoff data. Performances of the models are first assessed using a monthly runoff time series simulation, and their abilities to replicate runoff at different return periods were evaluated. Their performances are further evaluated using a set of transferrable benchmarks. Generally, different metrics can assess individual characteristics of a simulated time series (Burgan and Aksoy,

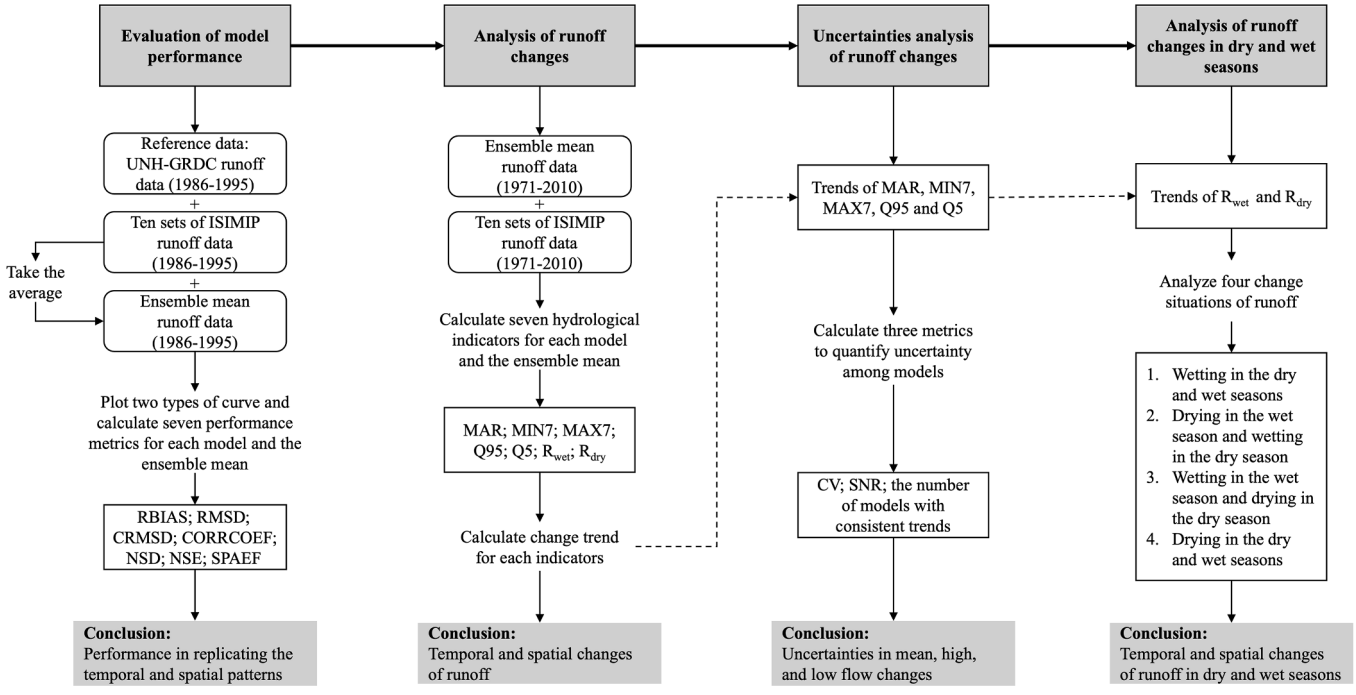


**Fig. 2.** The methodological outline of this study.

2022). In this study, seven metrics are applied to enable a comprehensive comparison. Six of these metrics (i.e., the relative bias, normalized root mean square difference (RMSD), correlation coefficient, normalized standard deviation (NSD), centered RMSD, and the Nash-Sutcliffe efficiency (NSE)) are applied to assess the relative performance of individual models in replicating the temporal patterns of reference runoff data. Their results are presented in three types of diagrams (the target diagram, the radar diagram, and the Taylor diagram). At the same time, the spatial efficiency metric (SPAEF) is adopted for spatial pattern comparison of the simulated and reference runoff data, which was originally proposed by Demirel et al. (2013). The expressions of each metric are presented in Table 2, and detailed evaluation criteria are also remarked in the table.

### 2.2.2. Hydrological indicators for runoff change

Seven hydrological indicators are employed to investigate the changes in the runoff regime within the LMRB for 1971–2010 (Table 3). Mean annual runoff (MAR), annual 7-day minima runoff (MIN7) and the annual 7-day maxima runoff (MAX7) are used to appraise the runoff regime changes relating to extreme events (Danneberg, 2012). The 95th percentile runoff (Q95) and the 5th percentile runoff (Q5) are applied to assess the low value and high value of runoff changes in the basin, respectively. Runoff in the wet season (Rwet) and runoff in the dry season (Rdry) are used to assess the overall runoff changes on an annual scale and during the wet and dry seasons, respectively. The hydrological indicators are calculated from the simulated daily runoff during the study period. Furthermore, to facilitate a comparison between the runoff changes identified by different models, the relative change trend in this study is expressed as the percentage change over the study period relative to the mean of the variable for each time series:

$$CR = \frac{k^* n}{\bar{x}} * 100 \quad (4)$$

where $CR$ represents the change ratio (%), $k$ (mm/year) is the estimated slope, $n$ is the number of years in the study period, and $\bar{x}$ is the mean of the analyzed variable.

A non-parametric estimation method using Sen's slope estimator is applied to each hydrological indicator to detect trends in runoff (Gilbert, 1987; Sen, 1968). As it estimates the trend of a time series based on the slope of the Kendall-Theil robust line (Theil, 1992), Sen's slope estimator is robust to outliers and has been widely used in studies to describe trend magnitudes in climate and hydrological variables (Stahl et al., 2012). In addition, Mann-Kendall's (Gilbert, 1987; Kendall, 1948; Mann, 1945) test at the significance level of 95% is also conducted to determine statistically significant trends in the long-term time series.

### 2.2.3. Metrics for quantifying uncertainty among models

Uncertainties relating to the multi-model analysis of changes in the runoff trend detection are quantified by using the coefficient of variation (CV), signal-to-noise ratio (SNR), and the number of models that agreed on the same trend of the model ensemble mean. CV is computed for the change trend in hydrological indicators estimated by the models, demonstrating the extent of variability in model estimates in relation to the mean. A higher CV indicates higher uncertainties and lower consistency between model estimates of runoff trend detection and vice versa. SNR is computed as the ratio between the external and internal variance for multi-model runoff simulations, providing the signal-to-noise levels by relating the ensemble's variance to that of the individual members' (Schellekens et al., 2017). Smaller SNR values represent higher uncertainties and lower consistency between model simulations of runoff. An SNR value below 1 indicates that the inter-model variability is larger than the ensemble mean variability, implying a low inter-model agreement for the runoff simulation. The number of models agreeing on the same trend of the model ensemble mean is then determined to reveal consistencies between the trend signs of the models.

**Table 2**
Description of seven metrics used in model performance evaluation.

| Metrics | Expression | Range | Remarks |
|---|---|---|---|
| Relative Bias | $RBIAS = \frac{\sum_{n=1}^{N}(S_n - O_n)}{\sum_{n=1}^{N} O_n} \times 100$ | $(-\infty, \infty)$ | *RBIAS* approaching 0 shows better performance |
| Correlation Coefficient | $\alpha = \frac{\sum_{n=1}^{N}(S_n - \overline{S})(O_n - \overline{O})}{\sqrt{\sum_{n=1}^{N}(S_n - \overline{S})^2}\sqrt{\sum_{n=1}^{N}(O_n - \overline{O})^2}}$ | $[-1, 1]$ | $\alpha$ approaching 1 shows better performance |
| Normalized Standard Deviation | $NSD = \frac{\sigma_s}{\sigma_o}$ | $[0, \infty)$ | *NSD* approaching 1 shows better performance |
| Normalized Root Mean Square Difference | $NRMSD = \frac{RMSD}{\sigma_s}$ | $[0, 1]$ | *NRMSD* approaching 0 shows better performance |
| Centered Root Mean Square Difference | $CRMSD = \sqrt{\frac{\sum_{n=1}^{N}((S_n - \overline{S}) - (O_n - \overline{O}))^2}{N}}$ | $[0, \infty)$ | *CRMSD* approaching 0 shows better performance |
| Nash-Sutcliffe Efficiency | $NSE = 1 - \frac{\sum_{n=1}^{N}(O_n - S_n)^2}{\sum_{n=1}^{N}(O_n - \overline{O})^2}$ | $(-\infty, 1]$ | *NSE* approaching 1 shows better performance |
| Spatial Efficiency Metric | $SPAEF = 1 - \sqrt{(\alpha - 1)^2 + (\beta - 1)^2 + (\gamma - 1)^2}$ | $(-\infty, 1]$ | *SPAEF* approaching 1 shows better performance |

Note: $S_n$ is the simulated value for the $n^{th}$ observation, $O_n$ is the observed value for the $n^{th}$ observation, the overall mean of $S$ and $O$ is indicated by an overbar ($\overline{S}$ and $\overline{O}$), $N$ is the sample size. $\sigma_s$ is the standard deviation of the simulated value, $\sigma_o$ is the standard deviation for the observation; $\alpha$ is the correlation coefficient; $\beta$ is the ratio of the coefficient of variation; $\gamma$ indicates the histogram overlap.

**Table 3**
Description of the seven hydrological indicators.

| Hydrological indicators | Description |
|---|---|
| MAR | Mean annual runoff for the period 1971–2010 |
| MIN7 | Sum of runoff during seven consecutive days where the total runoff is the minimum in a certain year |
| MAX7 | Sum of runoff during seven consecutive days where the total runoff is the maximum in a certain year |
| Q95 | Magnitude of the daily runoff that is exceeded 95% of the days in the time series, indicating low flow |
| Q5 | Magnitude of the daily runoff that is exceeded 5% of the days in the time series, indicating high flow |
| $R_{wet}$ | Total runoff for each year in the wet season (June–October) |
| $R_{dry}$ | Total runoff for each year in the dry season (November–May) |

## 3. Results

### 3.1. Evaluation of model performance

Performances of the ten selected models in simulating monthly runoff time series are evaluated against the reference data (UNH-GRDC runoff data) from 1986 to 1995 (Fig. 3a). Results show that all models could replicate the observed monthly runoff time series and the seasonal runoff cycles, and the multi-model ensemble mean agrees well with the reference data. The probability of exceedance of the model simulations was also investigated to assess the models' performances in simulating runoff at different return periods (Fig. 3b). Model simulated runoff is skewed differently at different magnitudes, and the models performed better in estimating the high flow than the low flow. Again, the model

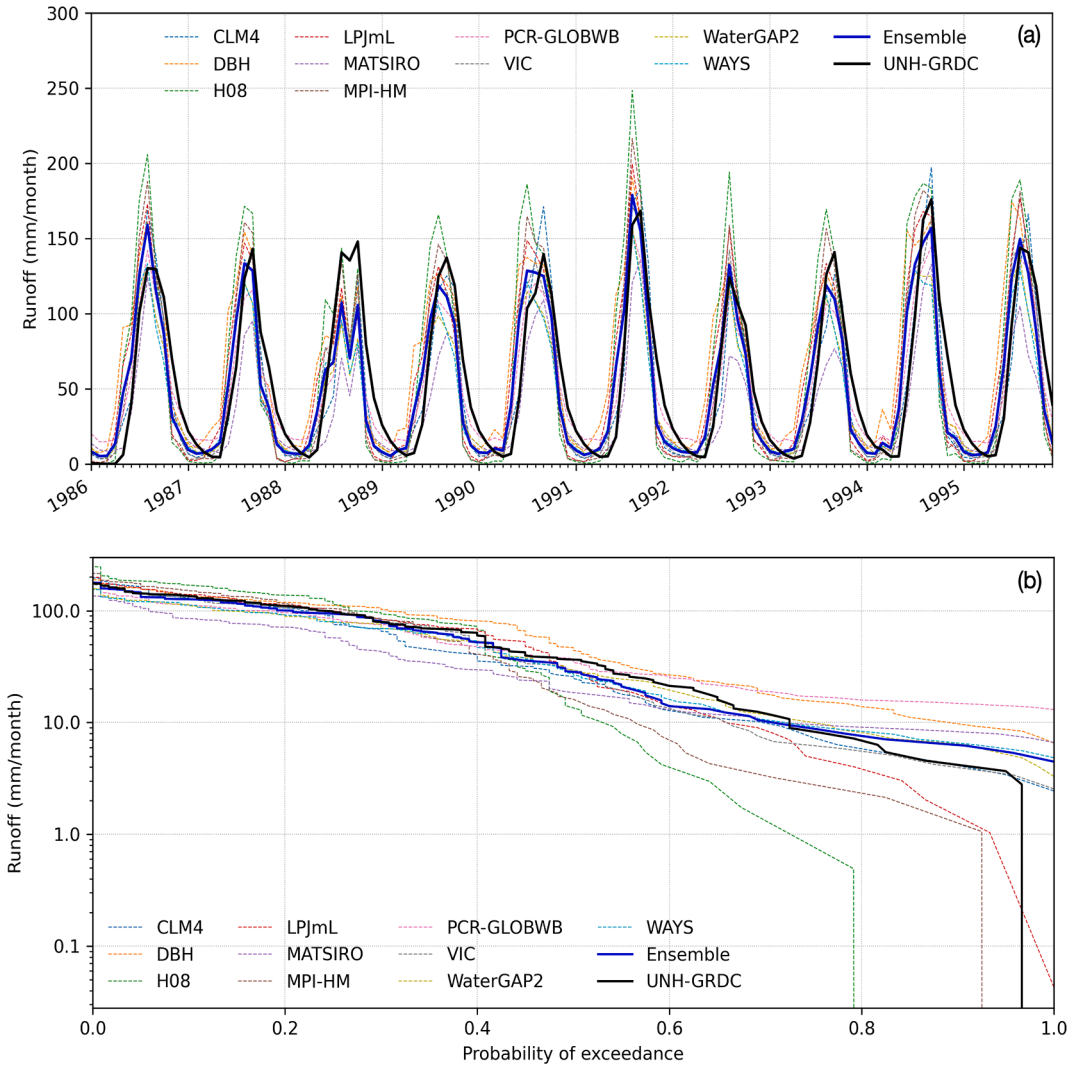


**Fig. 3.** Comparisons of the simulated monthly runoff time series by ISIMIP2a models with the UNH-GRDC runoff reference data during 1986–1995: (a) time series of the simulated runoff and (b) probability of exceedance of model simulated monthly runoff. The solid black line represents UNH-GRDC runoff reference data, the solid blue line represents the model ensemble mean, and the dashed lines represent ISIMIP2a model simulations. (For interpretation of the references to colour in this figure legend, the reader is referred to the web version of this article.)

ensemble mean resembles the exceedance probability well and provides a good match with the UNH-GRDC runoff data, indicating the high performance of the model ensemble mean of runoff at different magnitudes.

Fig. 4 displays the ten selected models' performance simulating monthly runoff time series. The relative bias between the reference data and model simulations is less than 10%, except for three models (DHB, H08, and MATSIRO). The relative bias is slightly higher but still below the threshold of ± 35% in these three models (Fig. 4a). The model ensemble mean exhibits the best relative bias score (2%) and the third-highest score in the normalized RMSD, indicating a generally good runoff simulation of the basin. The PCR-GLOBWB, CLM4, and the model ensemble mean exhibit better runoff simulation performances with smaller normalized RMSD values. In comparison, the performances of the DBH and H08 models are less favorable due to the relatively larger normalized RMSD. Most tested models demonstrate NSEs larger than 0.7, indicating good and highly accurate performances when reproducing the runoff time series. However, three models (H08, DBH, and LPJm) demonstrate low NSEs (Fig. 4b). The model ensemble mean achieves the best performance with an NSE value of 0.90, followed by WAYS (0.88), PCR-GLOBWB (0.88), and CLM4 (0.87).

The Taylor diagram depicts a comprehensive model-matching skill between simulated runoff and the reference runoff data (Fig. 4c). All models are found to have correlation coefficients higher than 0.8. Half of the models and the model ensemble mean have correlation coefficients greater than 0.9, exhibiting strong runoff simulation performances in this respect. Models with relatively high correlations typically have low normalized RMSD (Fig. 4c). A normalized standard deviation larger than one implies a somewhat higher variation in a model's simulated time series than the reference data. At the same time, values lower than one indicate that the time series has a weaker amplitude. Although the model simulations of CLM4, PCR-GLOBWB, and MATSIRO demonstrate stronger relationships with UNH-GRDC runoff data than the model ensemble mean, the model ensemble mean provides a better replication of the variations within the runoff time series, with the normalized standard deviation lying nearest to the green contour marked "Ref".

The results of the spatial performance evaluation are shown in Fig. 5. Compared with the reference runoff data, the model ensemble mean shows the best performance of high correlation, coefficient of variation, and histogram overlap. Most areas present high positive values with a mean SPAEF value of 0.53. In addition, most tested models demonstrate SPAEF larger than 0.4, indicating high spatial similarity with UNH-GRDC runoff reference data. Among the models, LPJmL and WAYS have the best performance, while CLM4, MATSIRO, and WaterGAP2

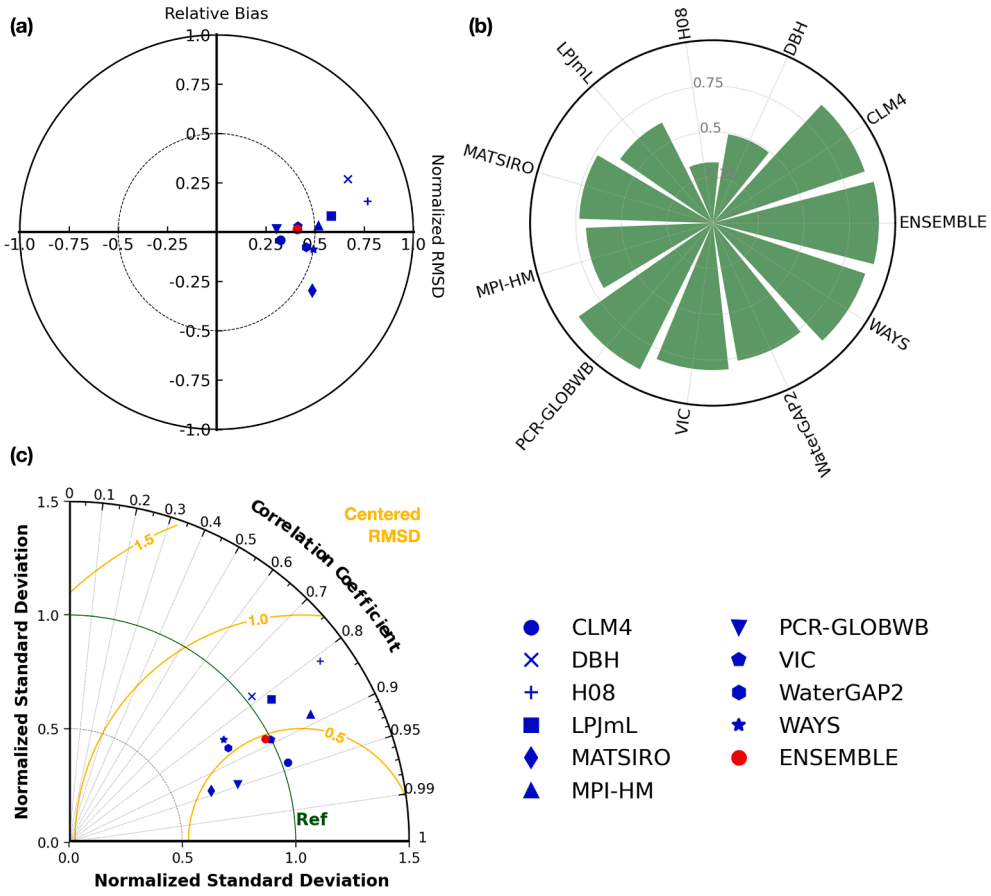


**Fig. 4.** Evaluation of the ten selected models' performance against the UNH-GRDC runoff reference data based on the (a) target diagram, (b) radar diagram, and (c) Taylor diagram during 1986–1995. The target diagram shows relative bias and normalized root mean square difference; the radar diagram shows the Nash-Sutcliffe efficiency; and the Taylor diagram shows the correlation coefficient, normalized standard deviation of errors, and centered root mean square difference.

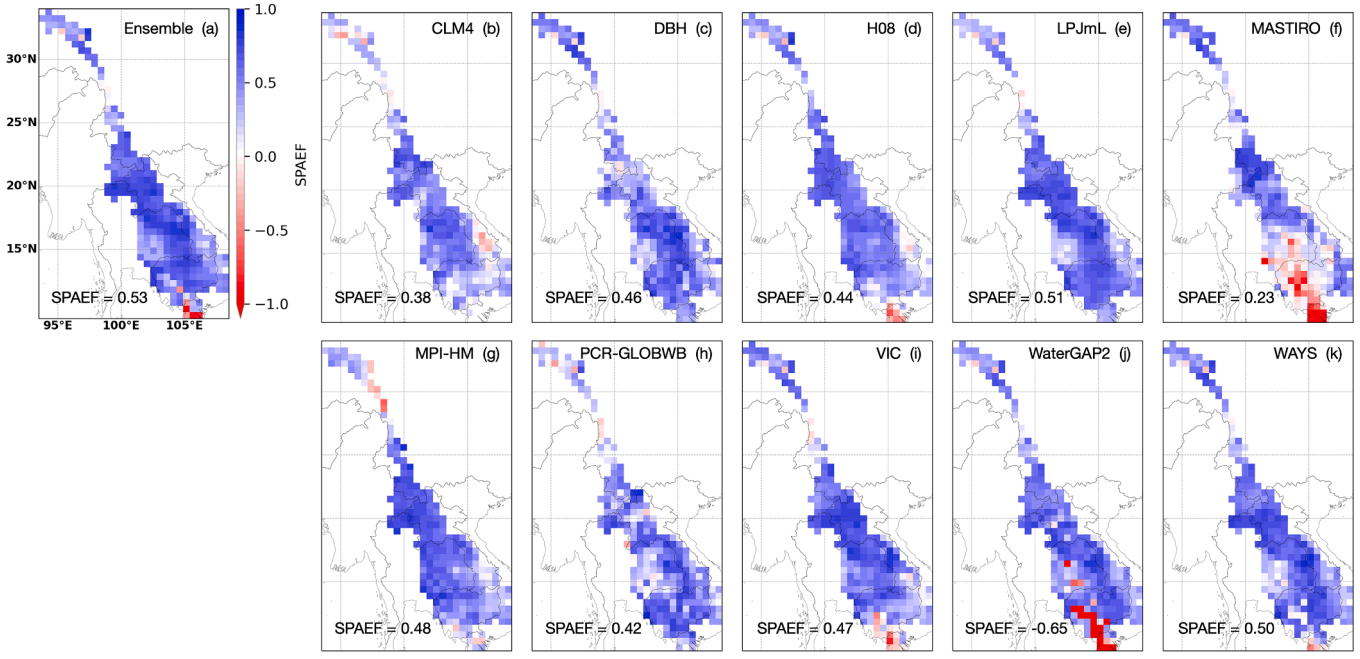


**Fig. 5.** Spatial efficiency (SPAEF) metric of (a) the model ensemble mean and (b-k) ISIMIP2a models during 1986–1995: (b) CLM4, (c) DBH, (d) H08, (e) LPJmL, (f) MATSIRO, (g) MPI-HM, (h) PCR-GLOBWB, (i) VIC, (j) WaterGAP2 and (k) WAYS. The mean SPAEF of all rasters is given in the lower left corner of each map.

demonstrate relatively low SPAEF, primarily located at the lower basin.

Overall, the above model evaluations reveal that the model ensemble mean outperforms the individual models for replicating monthly time series, seasonal cycles, and runoff at different return periods. Furthermore, the model ensemble mean is capable of modeling variability in the runoff time series, and shows the best spatial correlation with the UNH-GRDC runoff reference data. Therefore, the model ensemble mean is used to analyze runoff regime changes in the LMRB, and then the model-associated uncertainties are quantified based on the ten model simulations in the following sections.

### 3.2. Overall runoff regime changes on the basin scale

The MAR changes from the ten GHMs for 1971–2010 are depicted in Fig. 6a. The spread of the MAR simulations from the ten models indicates uncertainties in the model simulations. However, they show similar variabilities over the years. Based on the model ensemble mean, the annual MAR in the LMRB shows high interannual variability with an average annual value of 655 mm/yr. Over the study period, the ensemble mean MAR was of low value in 1977 (498.78 mm/yr) and 1998 (509.86 mm/yr), while it was of high value in 1978 (792.02 mm/yr) and 2000 (867.15 mm/yr). Overall, the MAR slightly increased by 52.61 mm (8.03%, $p$ greater than 0.05) from 1971 to 2010.

Fig. 6b depicts the estimated changes in the seven hydrological indicators from the ten GHMs for the LMRB in 1971–2010. Based on the multi-model simulation, all hydrological indicators demonstrate increasing change trends for the LMRB, except for MIN7 and Q95 indicators. Models also show relatively high agreements for change trend detections of MAR, MAX7, Q5, and $R_{wet}$ indicators. The highest model agreement is observed for the MAR trend detection, with the smallest spread range among the model estimates. In contrast, large uncertainties in model estimates are observed for change trend detections of low runoff values (MIN7 and Q95) and $R_{dry}$. The $R_{dry}$, in particular, ranged from 7.58% to 34.91%.

Overall, the model ensemble mean based estimates indicate that runoff in the LMRB had insignificantly increased during 1971–2010 in terms of low flows, high flows, MAR, and runoff in both dry and wet seasons. The change in the high flow, including MAR (8.14%), MAX7 (8.46%), and Q5 (8.03%), all exhibit insignificant increasing trends. The modeled low flow (MIN7 and Q95) has the lowest increasing ratio of the 2.23% and 1.67%, respectively. Runoff during the dry season shows the most significant increase (17.74%, $p > 0.05$), while runoff during the wet season increases slightly (approximately 6.24%, $p > 0.05$).

### 3.3. Spatial patterns in runoff changes and uncertainties

Fig. 7 illustrates the spatial patterns of change trends based on the model ensemble mean of MAR, low flow (MIN7 and Q95), and high flow (MAX7 and Q5) during 1971–2010. The spatial distribution of trend in MAR (Fig. 7a) is characterized by a prominent gradient from the upper and lower basin to the middle basin, with a strong increasing trend in the upper and lower basin that contradicts a predominantly decreasing trend in the middle basin and within a small region of the lower basin. The trends in high flow (Fig. 7c,e) exhibit broadly similar patterns to the trends in MAR, with significant positive trends in the lower basin. The trends in low flow (Fig. 7b,d) have more prominent negative trends evident in the middle and lower basins (but with lower local variability), which are slightly different from those of other hydrological indicators. In addition, the models demonstrate a general consistent trend detection for MAR, MAX7, and Q5 at most of the region. All the models show similar trends of the model ensemble mean (both positive and negative). However, there are more noticeable inconsistencies between the model estimates of MIN7 and Q95, and the disagreement among models is widespread across the upper and lower basin. Overall, the model simulations of runoff show a significant difference in spatial distribution, with better and more consistent performance in MAR and high runoff (MAX7 and Q5) than the low runoff (MIN7 and Q95).

Fig. 8 depicts the uncertainties associated with the model trend detection to evaluate the model consistency among the models further. As all models are driven by the same climate forcings, the uncertainties are only related to differences between the model structures and parameters. The uncertainty analysis of MAR indicates high agreements for estimating trend magnitudes across the basin, where the CV is lower than 50% for most regions (Fig. 8a). Grid cells with relatively high disagreement are sparsely distributed in the upper-most, middle, and lower-most areas. The models are strongly consistent when detecting the trend signal (Fig. 7a) in either positive or negative regions (Fig. 8k). For most areas, all models demonstrate the same change trend signal of the model ensemble mean, indicating the high performance of models in estimating the runoff. Although high consistency is observed in estimating the MAR trend signal and magnitude, the SNR results also show that some regions (upper basin and the western part of the lower basin) have more significant inter-model variability than the ensemble mean, indicating a large spread in the runoff simulation among models (Fig. 8f).

Uncertainties in high flow (Q5 and MAX7) are found to have generally similar patterns with the MAR in terms of CV and model agreements with the trend signal, even though the local variability differed slightly (Fig. 8c,e). There are large differences in the SNR between MAR and high flow (Fig. 8h,j). MAX7 demonstrates a high inter-model agreement in the runoff simulation across the entire basin, except for a small region in the upper and lower basin. In contrast, Q5 generally demonstrates a low inter-model agreement within the LMRB, and only a few middle and lower basin areas exhibit lower uncertainties. However,

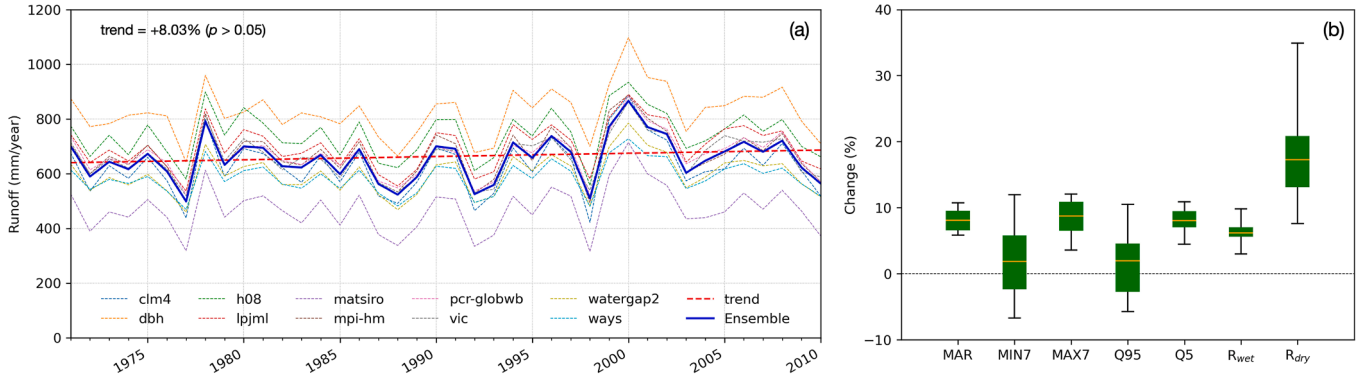


**Fig. 6.** Time series of changes in MAR and box-whiskers of changes in the seven hydrological indicators in the LMRB during 1971–2010: (a) MAR time series showing the change trend; (b) The box-whiskers represent the 25th, 50th, and 75th percentiles of the distribution in changes for each hydrological indicator (all the trends are not significant).

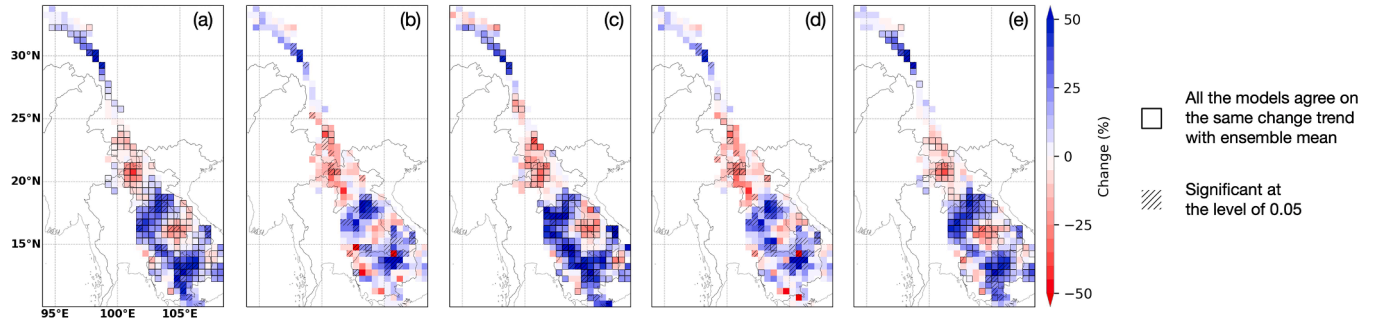


**Fig. 7.** Spatial distribution of change trends in five hydrological indicators based on the model ensemble mean from ten selected models in the LMRB during 1971–2010: (a) mean annual runoff, (b) annual 7-day minima runoff, (c) annual 7-day maxima runoff, (d) 95th percentile runoff, and (e) 5th percentile runoff.

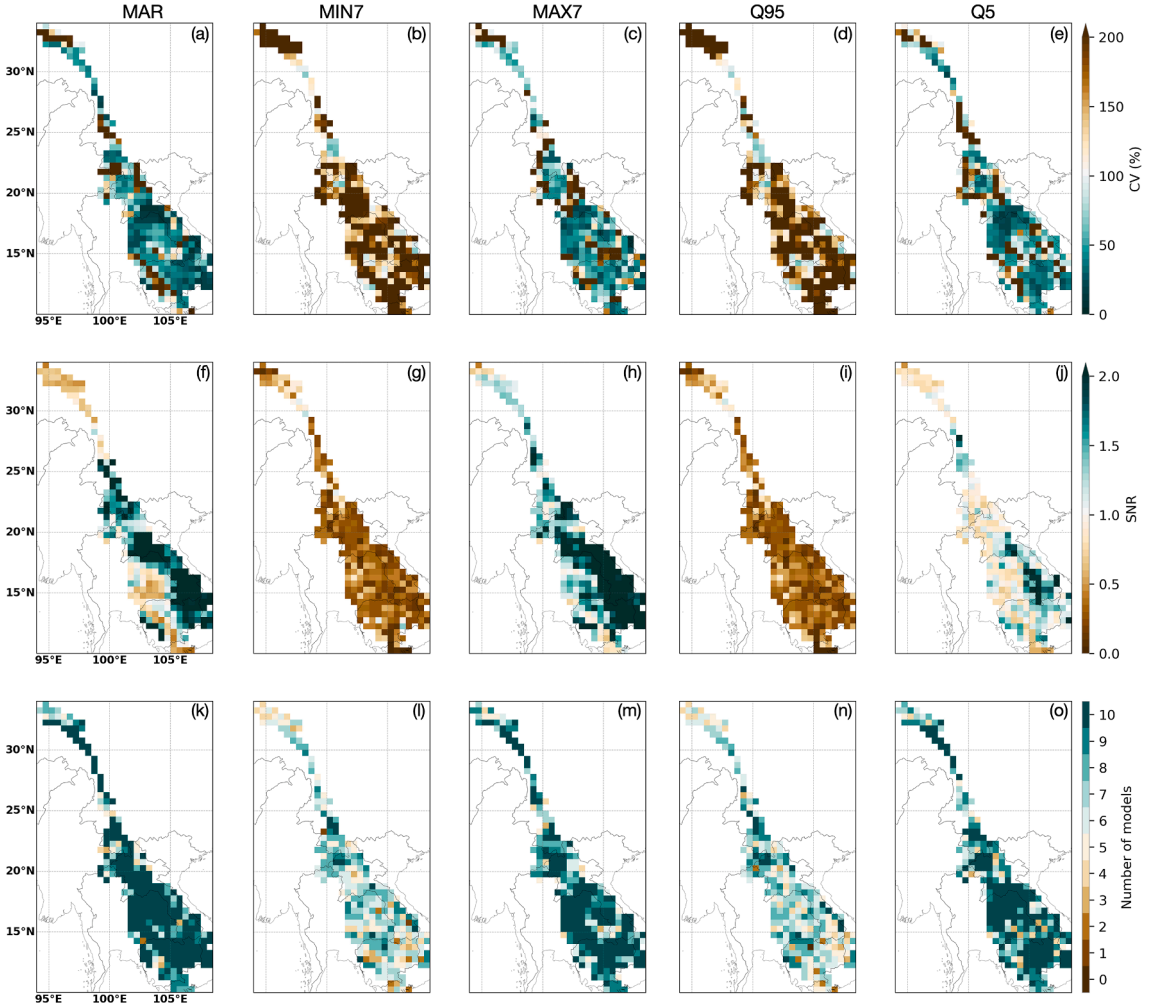


**Fig. 8.** Uncertainties in multi-model runoff trend detection quantified by (a-e) the coefficient of variation (CV) and (f-j) signal-to-noise ratio (SNR), and (k-o) the number of models that agree with the same trend as the model ensemble mean. The hydrological indicators include the mean annual runoff (MAR, a, f, k), annual 7-day minima runoff (MIN7, d, g, l), annual 7-day maxima runoff (MAX7, c, h, m), 95th percentile runoff (Q95, b, i, n), and 5th percentile runoff (Q5, e, j, o). To facilitate a comparison between the different uncertainty indicators, brown indicates low consistency and large uncertainty and cyan indicates high consistency and small uncertainty. (For interpretation of the references to colour in this figure legend, the reader is referred to the web version of this article.)

the low flow (Q95 and MIN7) clearly shows different patterns compared to MAR and high flow for all the agreement metrics (Fig. 8b,d,g,i,l,n). There were large disagreements in the runoff simulations between the models over the entire basin, with the CV value larger than 200% and the SNR value lower than 1. In addition, the number of models that are consistent with the trend in the model ensemble mean is less at low flow than at high flow (Fig. 8l,n). Overall, MAR, MAX7 and Q5 exhibit high consistency and low uncertainties between the models, indicating that the model estimates of the annual runoff and high flow changes are more accurate. However, MIN7 and Q95 express relatively low consistency and high uncertainties among the models.

### 3.4. Runoff changes in dry and wet seasons

Strongly influenced by the Indian monsoon and the East Asian monsoon, the LMRB has distinct dry and wet seasons (Pokhrel et al., 2018a). Therefore, the runoff change trend is also investigated in the LMRB for the dry and wet seasons. The model ensemble mean shows that runoff has increased by 6.04% in the wet season and 16.6% in the dry season. The runoff change trend detection of individual models is depicted in Fig. 9. All models demonstrate increasing runoff trends in dry and wet seasons but with different magnitudes. The runoff trends simulated by the models ranged from 3% to 9.83% in the wet season, and 7.58% to 34.91% in the dry season. Among the ten models, only PCR-GLOBWB demonstrates a significant increasing trend in the dry season, which is insignificant for other models. Additionally, the estimated monthly average runoff varied from 70.85 mm/month to 132.22 mm/month in the wet season, between 13.49 mm/month and 40.22 mm/month in the dry season.

Spatially, the runoff changes in the wet and dry seasons demonstrate similar patterns throughout the basin, except for some small areas in the middle and lower basin (Fig. 10a,b). In the dry season (Fig. 10b), the areas in the middle basin that demonstrate a decreasing trend are considerably more prominent than in the wet season, and the magnitude of the trend is also relatively higher. In the center of the lower basin, increasing runoff trends are observed in the dry season (Fig. 10b), and opposite decreasing trends are observed in the wet season (Fig. 10a). The increasing trend in the dry season is significant in larger areas than in the wet season. The results also show high model consistency for the trend signal in both dry and wet seasons, as shown by the grid cells with the box.

The LMRB has experienced droughts and floods in recent decades (Pokhrel et al., 2018b). The increases and decreases in runoff in the wet and dry seasons, respectively, enhance the wet and dry conditions in the region. Fig. 10c highlights the areas with different change patterns, identified by investigating the spatial characteristics of runoff changes in the dry and wet seasons. In general, 30% of the area within the basin becomes drier in the dry season (red and yellow pixels in Fig. 10c). On the other hand, about 70% of the area becomes wetter in the wet season (green and blue pixels in Fig. 10c). 17% of the region (yellow pixels in Fig. 10c) suffers from both situations and becomes drier in the dry seasons and wetter in the wet seasons. Furthermore, some areas exhibited decreased runoff in the wet season and increased runoff in the dry season (green pixels in Fig. 10c).

## 4. Discussion

This study examines the runoff changes in the LMRB for 1971–2010 using ten hydrological models from the ISIMIP. Different indicators are applied to provide a deeper analysis of the historical runoff regime change and uncertainties relating to the multi-model simulations. Overall, model evaluations show that all models could replicate the temporal and spatial variability of the reference runoff well (Figs. 2-4). Regarding temporal variability, WAYS, PCR-GLOBWB, and CLM4 have the best performance among the models (Figs. 3, 4). For spatial variability, LPJmL and WAYS are the best, with high correlation, coefficient of variation and histogram overlap with the reference data (Fig. 5). As the same climate forcings drive all models, these varied performances can be related to the differences between the model structures and parameters, i.e., snowmelt scheme, evapotranspiration scheme, number of soil layers, etc. (Chen et al., 2021; Gudmundsson et al., 2012). However, the uncertainty in climate forcing should not be neglected, which introduced uncertainty in the simulation outputs (Biemans et al., 2009). Furthermore, the low spatial performance in the areas close to the estuary may be sourced from the missing effects of interactions between sea and river, which could significantly influence the hydrological processes (Chen et al., 2021; Pokhrel et al., 2018). Generally, there is lower variability among the models for mean and high flow than low flow (Fig. 8), suggesting higher uncertainty when simulating trends under dry conditions. These results are consistent with Zaherpour et al. (Beck et al., 2017), who evaluated extreme runoff simulations by six hydrological models in most basins worldwide, including the LMRB. Such uncertainty may be attributed to low flow being more sensitive to model structure and parameters than other uncertainty sources (Chen et al., 2021; Zaherpour et al., 2018). Our results also reveal that the model ensemble mean outperforms the individual models for replicating the reference runoff data at both temporal and spatial scales (Figs. 3-5); similar results are found in previous model evaluations (e.g., Chen et al., 2021; Gudmundsson et al., 2012), which may be due to the reduced uncertainties of the different model structures and parameterizations when averaging the model outputs (Reichler and Kim, 2008).

Regarding the trend of runoff in the LMRB over the study period, the runoff trend is not significant on the basin scale. Still, it is significant in many areas, suggesting a highly spatially heterogenous runoff change across the LMRB. Although there is an insignificant positive trend in MAR of 8.03% on a basin scale (Fig. 6a), large areas in the middle basin have demonstrated negative trends of the mean, high and low flow (Fig. 7). This agrees with the study of Lu and Siew (2014), who found that the observed discharge in the station of Luang Prabang, located in the middle stream, has decreased since 1960. In addition, the center of the lower basin is another hotspot area with negative runoff trends. Such area with pronounced decreasing runoff trends was rarely reported in studies before Wang et al. (2020), who investigated the possible reasons for changes in inundation within the Tonle Sap Lake. They found that the significant decrease in the lake area since 2000 is mainly due to decreased precipitation in the middle basin. This area is consistent with

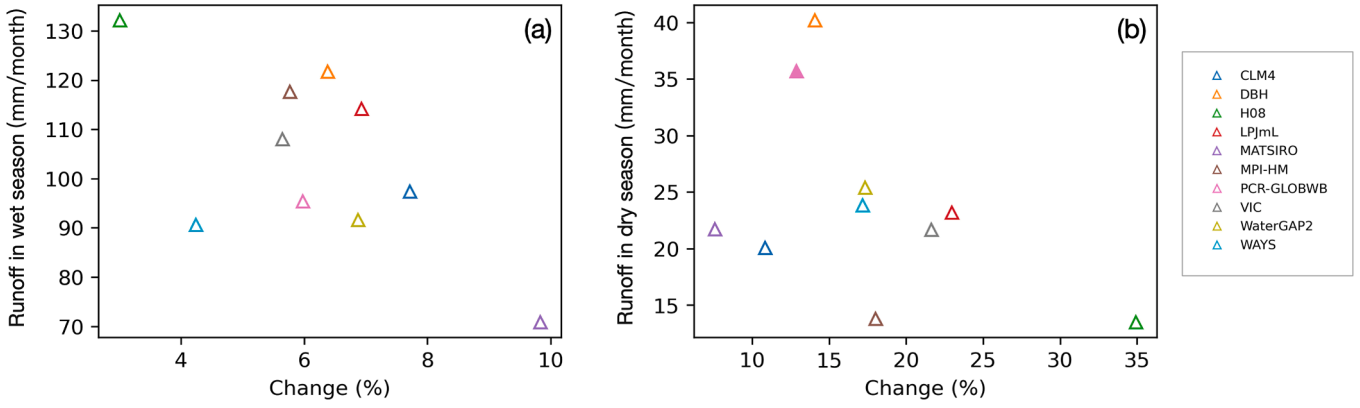


**Fig. 9.** Runoff changes in (a) wet and (b) dry seasons for individual models during 1971–2010. The filled triangle shows that the trend is significant at the 0.05 significance level.

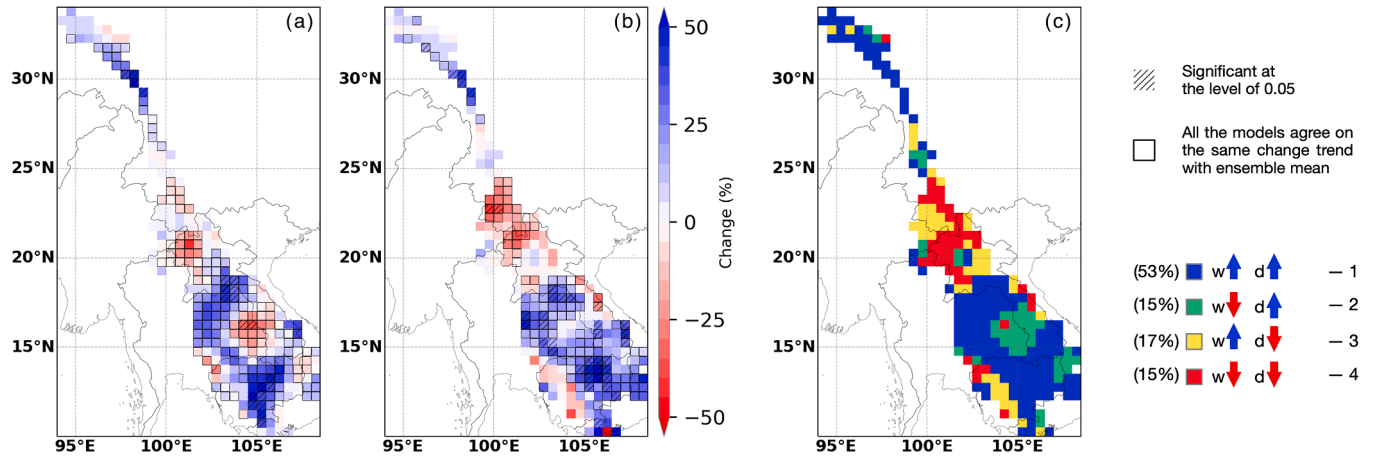


**Fig. 10.** Spatial distribution of runoff trends in (a) wet and (b) dry seasons based on the model ensemble mean during 1971–2010. Grid cells with diagonal lines indicate significant trends at the 0.05 significance level, and boxes with pixels indicate that all the models shared the same trend signal as the model ensemble mean. Runoff regime change in the LMRB from 1971 to 2010 based on four different change situations (c): (1) wetting in the dry and wet seasons, (2) drying in the wet season and wetting in the dry season, (3) wetting in the wet season and drying in the dry season, and (4) drying in the dry and wet seasons.

the hotspot region identified in our study (Fig. 7).

The sophisticated map of four different change situations in the basin (Fig. 10c) is crucial for enabling accurate water management practices in the LMRB. Approximately 70% of the region within the basin experiences increased runoff during the wet season, mainly in the upper and lower basin. In the middle basin, the amount of runoff has declined in the dry season, thereby may push more local water stress, particularly for irrigation for agriculture (Lu et al., 2014). However, the basin with an increased runoff trend in the dry season can provide irrigation to crops and reduce the intrusion of Mekong Delta seawater in the basin, particularly in the dry season (Ziv et al., 2012). Our study also reveals that runoff in approximately 15% of the basin has increased in the dry season but declined in the wet season. In such regions, their water stress during dry periods and flood risk during wet periods may be alleviated. The Tonle Sap Lake located in this area is evident to experience reduced (increased) water surface in the wet (dry) season, which may have critical implications for the local fishery that is sensitive to the water level of Tonle Sap Lake (Chen et al., 2021; Wang et al., 2020). It is also important to note that 17% of the basin domain has become wetter in the wet season and drier in the dry season, which may increase local water management pressures, requiring attention for water crises.

There are limitations to this study. First, the trends derived by models are forced by only one single dataset, implying that the uncertainties associated with the input were not investigated. Moreover, this study is conducted using the period 1971–2010, and it is acknowledged that any trend calculation depends strongly on the selection period, as highlighted in many previous studies. Thus, further work is required to investigate whether the relatively short period selected (40 years in this study) is representative of variability in the long term. Furthermore, the current study focuses only on the change trends of historical runoff. A more comprehensive study that considers both human activities and climate change would thus be more beneficial for identifying the causes of changes in the runoff regime.

## 5. Conclusion

This study applies a multi-model framework to investigate historical temporal-spatial runoff regime changes in the LMRB during 1971–2010 for the first time, and the spatial characteristics and uncertainties are also analyzed. The main conclusions can be summarized as follows:

1. All ten models from ISIMIP2a can replicate the temporal and spatial patterns of the reference data but with different performances. The model ensemble mean outperforms the individual models for replicating the reference runoff data at both temporal and spatial scales.
2. The models better simulate the annual runoff and high flow changes than the low flow, with higher consistencies and lower uncertainties of the annual runoff and high flow between the models.
3. The annual runoff in the LMRB shows an insignificantly positive trend (8.03%) during 1971–2010, with a higher increase of high flow (MAX7 (8.46%), and Q5 (8.03%)) than low flow (MIN7 (2.23 %), and Q95 (1.67%)).
4. The runoff trend is spatially heterogeneous across the LMRB. The trends in high flow exhibit broadly similar spatial patterns to the annual runoff, with significantly increasing trends in the lower basin. On the other hand, the low flow shows prominent decreasing trends in the middle and lower basins.
5. Considering the different runoff trends in the dry and wet seasons, about 32% (70%) of the basin became drier (wetter) in the dry (wet) season. Meanwhile, 17% of the basin experienced the dry season getting drier and the wet season getting wetter, which may increase local water management pressures.

Overall, the novelty of this study lies in the compilation of detailed analysis of temporal-spatial changes in the mean, high, and low flows, and the identification of the corresponding uncertainties. Such a thorough investigation of runoff regime changes provides crucial information for water resource management and risk mitigation in the LMRB. However, uncertainty analyses further suggest that attention should be paid when interpreting the results when cross-model consistency is low. Therefore, subsequent studies focusing on runoff should also consider areas with relatively large uncertainties.

## CRediT authorship contribution statement

**Yuxin Li:** Conceptualization, Methodology, Data curation, Formal analysis, Visualization, Writing – original draft, Writing – review & editing. **Aifang Chen:** Conceptualization, Formal analysis, Visualization, Writing – original draft, Writing – review & editing. **Ganquan Mao:** Conceptualization, Methodology, Visualization, Writing – original draft. **Penghan Chen:** Writing – review & editing. **Hao Huang:** Writing – review & editing. **Zifeng Wang:** Writing – review & editing. **He Chen:** Writing – review & editing. **Kai Wang:** Writing – review & editing. **Ying Meng:** Writing – review & editing. **Rui Zhong:** Writing – review & editing. **Pengfei Wang:** Writing – review & editing. **Junguo Liu:** Supervision, Funding acquisition, Writing - review & editing.

## Declaration of Competing Interest

The authors declare that they have no known competing financial interests or personal relationships that could have appeared to influence the work reported in this paper.

## Data availability

All the data used in this work are available at the "The Inter-Sectoral Impact Model Intercomparison Project" (ISIMIP, https://www.isimip.org)

## Acknowledgments

This study has been supported by the National Natural Science Foundation of China (Grant No. 41625001), the Strategic Priority Research Program of the Chinese Academy of Sciences (XDA20060402), the National Natural Science Foundation of China (Grant No. 42101025, 42101041), the China Postdoctoral Science Foundation (Grant No. 2021M691403), the Henan Provincial Key Laboratory of Hydrosphere and Watershed Water Security, and the SUSTech Presidential Postdoctoral Fellowship. We also acknowledge the Special Funds for the Cultivation of Guangdong College Students' Scientific and Technological Innovation ("Climbing Program"Special Funds) (pdjh2020c123456). All the data used in this work are available at the "The Inter-Sectoral Impact Model Intercomparison Project" (ISIMIP, https://www.isimip.org).

## Appendix A. Supplementary data

Supplementary data to this article can be found online at https://doi.org/10.1016/j.jhydrol.2023.129297.

## References

Alcamo, J., Döll, P., Henrichs, T., Kaspar, F., Lehner, B., Rösch, T., Siebert, S., 2003. Development and testing of the WaterGAP 2 global model of water use and availability. Hydrol. Sci. J. 48 (3), 317–337.

Asadieh, B., Krakauer, N., Fekete, B., 2016. Historical trends in mean and extreme runoff and streamflow based on observations and climate models. Water (Switzerland) 8 (5), 189.

Bawden, A.J., Burn, D.H., Prowse, T.D., 2015. Recent changes in patterns of western Canadian river flow and association with Climatic drivers. Hydrol. Res. 46, 551–565. https://doi.org/10.2166/nh.2014.032.

Beck, H.E., Van Dijk, A.I.J.M., De Roo, A., Dutra, E., Fink, G., Orth, R., Schellekens, J., 2017. Global evaluation of runoff from 10 state-of-the-art hydrological models. Hydrol. Earth Syst. Sci. 21, 2881–2903. https://doi.org/10.5194/hess-21-2881-2017.

Biemans, H., Hutjes, R.W.A., Kabat, P., Strengers, B.J., Gerten, D., Rost, S., 2009. Effects of precipitation uncertainty on discharge calculations for main river basins. J. Hydrometeorol. 10, 1011–1025. https://doi.org/10.1175/2008JHM1067.1.

Burgan, H.I., Aksoy, H., 2022. Daily flow duration curve model for ungauged intermittent subbasins of gauged rivers. J. Hydrol. 604, 127249 https://doi.org/10.1016/j.jhydrol.2021.127249.

Chen, H., Liu, J., Mao, G., Wang, Z., Zeng, Z., Chen, A., Wang, K., Chen, D., 2021. Intercomparison of ten ISI-MIP models in simulating discharges along the Lancang-Mekong River basin. Sci. Total Environ. 765, 144494 https://doi.org/10.1016/j.scitotenv.2020.144494.

Danneberg, J., 2012. Changes in runoff time series in Thuringia, Germany - Mann-Kendall trend test and extreme value analysis. Adv. Geosci. 31, 49–56.

Demirel, M.C., Booij, M.J., Hoekstra, A.Y., 2013. Effect of different uncertainty sources on the skill of 10 day ensemble low flow forecasts for two hydrological models. Water Resour. Res. 49, 4035–4053. https://doi.org/10.1002/wrcr.20294.

Eastham, J., Mpelasoka, F., Ticehurst, C., Dyce, P., Ali, R., Kirby, M., 2008. Mekong River Basin Water Resources Assessment: Impacts of Climate Change. CSIRO Water a Heal. Ctry. Flagsh. Rep, Ser, p. 153.

Fekete, B.M., Vorosmarty, C.J., HALL, F.G., COLLATZ, G.J., MEESON, B.W., LOS, S.O., BROWN DE COLSTOUN, E., LANDIS, D.R., 2011. ISLSCP II UNH/GRDC Composite Monthly Runoff. ORNL DAAC. https://doi.org/10.3334/ORNLDAAC/994.

Gerten, D., Schaphoff, S., Haberlandt, U., Lucht, W., Sitch, S., 2004. Terrestrial vegetation and water balance—hydrological evaluation of a dynamic global vegetation model. J. Hydrol. 286, 249–270. https://doi.org/10.1016/j.jhydrol.2003.09.029.

Gilbert, R.O., 1987. Statistical methods for environmental pollution monitoring. John Wiley & Sons.

Giuntoli, I., Vidal, J.P., Prudhomme, C., Hannah, D.M., 2015. Future hydrological extremes: The uncertainty from multiple global climate and global hydrological models. Earth Syst. Dyn. 6, 267–285. https://doi.org/10.5194/esd-6-267-2015.

Gosling, S.N., Arnell, N.W., 2011. Simulating current global river runoff with a global hydrological model: Model revisions, validation, and sensitivity analysis. Hydrol. Process. 25, 1129–1145. https://doi.org/10.1002/hyp.7727.

Gudmundsson, L., Wagener, T., Tallaksen, L.M., Engeland, K., 2012. Evaluation of nine large-scale hydrological models with respect to the seasonal runoff climatology in Europe. Water Resour. Res. 48, 1–20. https://doi.org/10.1029/2011WR010911.

Hanasaki, N., Kanae, S., Oki, T., Masuda, K., Motoya, K., Shirakawa, N., Shen, Y., Tanaka, K., 2008. An integrated model for the assessment of global water resources - Part 1: Model description and input meteorological forcing. Hydrol. Earth Syst. Sci. 12, 1007–1025.

Hasson, S., Pascale, S., Lucarini, V., Böhner, J., 2016. Seasonal cycle of precipitation over major river basins in South and Southeast Asia: A review of the CMIP5 climate models data for present climate and future climate projections. Atmos. Res. 180, 42–63. https://doi.org/10.1016/j.atmosres.2016.05.008.

Hattermann, F.F., Vetter, T., Breuer, L., Su, B., Daggupati, P., Donnelly, C., Fekete, B., Flörke, F., Gosling, S.N., Hoffmann, P., Liersch, S., Masaki, Y., Motovilov, Y., Müller, C., Samaniego, L., Stacke, T., Wada, Y., Yang, T., Krysnaova, V., 2018. Sources of uncertainty in hydrological climate impact assessment: a cross-scale study. Environ. Res. Lett. 13, 15006. https://doi.org/10.1088/1748-9326/aa9938.

Hoang, L.P., van Vliet, M.T.H., Kummu, M., Lauri, H., Koponen, J., Supit, I., Leemans, R., Kabat, P., Ludwig, F., 2019. The Mekong's future flows under multiple drivers: How climate change, hydropower developments and irrigation expansions drive hydrological changes. Sci. Total Environ. 649, 601–609. https://doi.org/10.1016/j.scitotenv.2018.08.160.

M.G. Kendall Rank correlation methods., Rank correlation methods 1948 Griffin, Oxford, England.

Lauri, H., De Moel, H., Ward, P.J., Räsänen, T.A., Keskinen, M., Kummu, M., 2012. Future changes in Mekong River hydrology: Impact of climate change and reservoir operation on discharge. Hydrol. Earth Syst. Sci. 16, 4603–4619. https://doi.org/10.5194/hess-16-4603-2012.

Lawrence, D.M., Oleson, K.W., Flanner, M.G., Thornton, P.E., Swenson, S.C., Lawrence, P.J., Zeng, X., Yang, Z.-L., Levis, S., Sakaguchi, K., Bonan, G.B., Slater, A.G., 2011. Parameterization improvements and functional and structural advances in Version 4 of the Community Land Model. J. Adv. Model. Earth Syst. 3 (1), n/a–n/a.

Liang, X., Lettenmaier, D.P., Wood, E.F., Burges, S.J., 1994. A simple hydrologically based model of land surface water and energy fluxes for general circulation models. J. Geophys. Res. 99, 14415–14428.

Liu, J., Chen, D., Mao, G., Irannezhad, M., Pokhrel, Y., 2022. Past and Future Changes in Climate and Water Resources in the Lancang-Mekong River Basin: Current Understanding and Future Research Directions. Engineering 13, 144–152.

Lu, X.X., Li, S., Kummu, M., Padawangi, R., Wang, J.J., 2014. Observed changes in the water flow at Chiang Saen in the lower Mekong: Impacts of Chinese dams? Quat. Int. 336, 145–157. https://doi.org/10.1016/j.quaint.2014.02.006.

Lyon, S.W., King, K., Polpanich, O., uma, Lacombe, G.,, 2017. Assessing hydrologic changes across the Lower Mekong Basin. J. Hydrol. Reg. Stud. 12, 303–314. https://doi.org/10.1016/j.ejrh.2017.06.007.

Mann, H.B., 1945. Non-parametric tests against trend. Econometrica 13, 245–259.

Mao, G., Liu, J., 2019. WAYS v1: a hydrological model for root zone water storage simulation on a global scale. Geosci. Model Dev. 12, 5267–5289. https://doi.org/10.5194/gmd-12-5267-2019.

Marx, A., Kumar, R., Thober, S., Zink, M., Wanders, N., Wood, E., Ming, P., Sheffield, J., Samaniego, L., 2017. Climate change alters low flows in Europe under a 1.5, 2, and 3 degree global warming. Hydrol. Earth Syst. Sci. Discuss. 1–24. https://doi.org/10.5194/hess-2017-485.

Masaki, Y., Hanasaki, N., Biemans, H., Schmied, H.M., Tang, Q., Wada, Y., Gosling, S.N., Takahashi, K., Hijioka, Y., 2017. Intercomparison of global river discharge simulations focusing on dam operation - Multiple models analysis in two case-study river basins. Missouri-Mississippi and Green-Colorado. Environ. Res. Lett. 12 (5), 055002.

Milly, P.C.D., Dunne, K.A., Vecchia, A.V., 2005. Global pattern of trends in streamflow and water availability in a changing climate. Nature 438, 347–350. https://doi.org/10.1038/nature04312.

Najafi, M.R., Moradkhani, H., 2015. Multi-model ensemble analysis of runoff extremes for climate change impact assessments. J. Hydrol. 525, 352–361. https://doi.org/10.1016/j.jhydrol.2015.03.045.

Phi Hoang, L., Lauri, H., Kummu, M., Koponen, J., Vliet, M.T.H.V.H. Van, Supit, I., Leemans, R., Kabat, P., Ludwig, F., Hoang, L.P., Lauri, H., Kummu, M., Koponen, J., Vliet, M.T.H.V.H. Van, Supit, I., Leemans, R., Kabat, P., Ludwig, F., 2016. Mekong River flow and hydrological extremes under climate change. Hydrol. Earth Syst. Sci. 20, 3027–3041. https://doi.org/10.5194/hess-20-3027-2016.

Phi Hoang, L., Lauri, H., Kummu, M., Koponen, J., Vliet, M.T.H.V., Supit, I., Leemans, R., Kabat, P., Ludwig, F., 2016. Mekong River flow and hydrological extremes under climate change. Hydrol. Earth Syst. Sci. 20, 3027–3041. https://doi.org/10.5194/hess-20-3027-2016.

Pokhrel, Y., Burbano, M., Roush, J., Kang, H., Sridhar, V., Hyndman, D., 2018a. A Review of the Integrated Effects of Changing Climate, Land Use, and Dams on Mekong River Hydrology. Water 10, 266. https://doi.org/10.3390/w10030266.

Pokhrel, Y., Shin, S., Lin, Z., Yamazaki, D., Qi, J., 2018b. Potential Disruption of Flood Dynamics in the Lower Mekong River Basin Due to Upstream Flow Regulation. Sci. Rep. 8, 17767. https://doi.org/10.1038/s41598-018-35823-4.

Reichler, T., Kim, J., 2008. How well do coupled models simulate today's climate? Bull. Am. Meteorol. Soc. 89, 303–311. https://doi.org/10.1175/BAMS-89-3-303.

Schellekens, J., Dutra, E., Martínez-De La Torre, A., Balsamo, G., Van Dijk, A., Sperna Weiland, F., Minvielle, M., Calvet, J.C., Decharme, B., Eisner, S., Fink, G., Flörke, M., Peßenteiner, S., Van Beek, R., Polcher, J., Beck, H., Orth, R., Calton, B., Burke, S., Dorigo, W., Weedon, G.P., 2017. A global water resources ensemble of hydrological models: The eartH2Observe Tier-1 dataset. Earth Syst. Sci. Data 9, 389–413. https://doi.org/10.5194/essd-9-389-2017.

Sen, P.K., 1968. Estimates of the Regression Coefficient Based on Kendall's Tau. J. Am. Stat. Assoc. 63, 1379–1389. https://doi.org/10.1080/01621459.1968.10480934.

Shan, C., Dong, Z., Huang, D., Lu, Y., Xu, W., Zhang, Y., 2021. Study on runoff evaluation law in the Luanhe River Basin. China. Polish J. Environ. Stud. 30, 361–368. https://doi.org/10.15244/pjoes/120350.

Sood, A., Smakhtin, V., 2015. Global hydrological models: a review. Hydrol. Sci. J. 60, 549–565. https://doi.org/10.1080/02626667.2014.950580.

Stacke, T., Hagemann, S., 2012. Development and evaluation of a global dynamical wetlands extent scheme. Hydrol. Earth Syst. Sci. 16, 2915–2933. https://doi.org/10.5194/hess-16-2915-2012.

Stahl, K., Tallaksen, L.M., Hannaford, J., Van Lanen, H.A.J., 2012. Filling the white space on maps of European runoff trends: Estimates from a multi-model ensemble. Hydrol. Earth Syst. Sci. 16, 2035–2047. https://doi.org/10.5194/hess-16-2035-2012.

Takata, K., Emori, S., Watanabe, T., 2003. Development of the minimal advanced treatments of surface interaction and runoff. Glob. Planet. Change 38, 209–222. https://doi.org/10.1016/S0921-8181(03)00030-4.

Tang, Q., Oki, T., Kanae, S., 2006. A distributed biosphere hydrological model (DBHM) for large river basin. Proc. Hydraul. Eng. 50, 37–42. https://doi.org/10.2208/prohe.50.37.

Tangdamrongsub, N., Han, S.-C., Decker, M., Yeo, I.-Y., Kim, H., 2018. On the use of the GRACE normal equation of inter-satellite tracking data for estimation of soil moisture and groundwater in Australia. Hydrol. Earth Syst. Sci. 22, 1811–1829. https://doi.org/10.5194/hess-22-1811-2018.

Theil, H., 1992. A rank-invariant method of linear and polynomial regression analysis, in: Henri Theil's Contributions to Economics and Econometrics. Springer, pp. 345–381.

Thompson, J.R., Green, A.J., Kingston, D.G., Gosling, S.N., 2013. Assessment of uncertainty in river flow projections for the Mekong River using multiple GCMs and hydrological models. J. Hydrol. 486, 1–30. https://doi.org/10.1016/j.jhydrol.2013.01.029.

van Beek, L.P.H., Wada, Y., Bierkens, M.F.P., 2011. Global monthly water stress: 1. Water balance and water availability. Water Resour. Res. 47, 15.

Västilä, K., Kummu, M., Sangmanee, C., Chinvanno, S., 2010. Modelling climate change impacts on the flood pulse in the lower mekong floodplains. J. Water Clim. Chang. 1, 67–86. https://doi.org/10.2166/wcc.2010.008.

Veldkamp, T.I.E., Wada, Y., Aerts, J.C.J.H., Döll, P., Gosling, S.N., Liu, J., Masaki, Y., Oki, T., Ostberg, S., Pokhrel, Y., Satoh, Y., Kim, H., Ward, P.J., 2017. Water scarcity hotspots travel downstream due to human interventions in the 20th and 21st century. Nat. Commun. 8, 15697. https://doi.org/10.1038/ncomms15697.

Wang, Y.e., Feng, L., Liu, J., Hou, X., Chen, D., 2020. Changes of inundation area and water turbidity of Tonle Sap Lake: Responses to climate changes or upstream dam construction? Environ. Res. Lett. 15 (9), 0940a1.

Warszawski, L., Frieler, K., Huber, V., Piontek, F., Serdeczny, O., Schewe, J., 2014. The inter-sectoral impact model intercomparison project (ISI-MIP): Project framework. Proc. Natl. Acad. Sci. U. S. A. 111, 3228–3232. https://doi.org/10.1073/pnas.1312330110.

Wu, Z., Chen, X., Lu, G., Xiao, H., He, H., Zhang, J., 2017. Regional response of runoff in CMIP5 multi-model climate projections of Jiangsu Province. China. Stoch. Environ. Res. Risk Assess. 31, 2627–2643. https://doi.org/10.1007/s00477-016-1349-9.

Yun, X., Tang, Q., Wang, J., Liu, X., Zhang, Y., Lu, H., Wang, Y., Zhang, L., Chen, D., 2020. Impacts of climate change and reservoir operation on streamflow and flood characteristics in the Lancang-Mekong River Basin. J. Hydrol. 590, 125472 https://doi.org/10.1016/j.jhydrol.2020.125472.

Zaherpour, J., Gosling, S.N., Mount, N., Müller Schmied, H., Veldkamp, T.I.E., Dankers, R., Eisner, S., Gerten, D., Gudmundsson, L., Haddeland, I., Hanasaki, N., Kim, H., Leng, G., Liu, J., Masaki, Y., Oki, T., Pokhrel, Y.N., Satoh, Y., Schewe, J., Wada, Y., 2018. Worldwide evaluation of mean and extreme runoff from six global-scale hydrological models that account for human impacts. Environ. Res. Lett. 13, 065015 https://doi.org/10.1088/1748-9326/aac547.

Ziv, G., Baran, E., Nam, S., Rodriguez-Iturbe, I., Levin, S.A., 2012. Trading-off fish biodiversity, food security, and hydropower in the Mekong River Basin. Proc. Natl. Acad. Sci. 109, 5609–5614. https://doi.org/10.1073/pnas.1201423109.